

CHALMERS
UNIVERSITY OF TECHNOLOGY

Domain Decomposition Analysis of Open-cavity-based Array Elements -- Roadmap Toward Analyzing Large-Scale Reflectarrays and Reconfigurable

Downloaded from: https://research.chalmers.se, 2026-11-11 07:21 UTC

Citation for the original published paper (version of record):
Maaskant, R., Lin, D., Maxharraj, F. et al (2025). Domain Decomposition Analysis of Open-cavity-based Array Elements -- Roadmap Toward Analyzing Large-Scale Reflectarrays and Reconfigurable Intelligent Surfaces. Proceedings of the International Conference on Electromagnetics in Advanced Applications, ICEAA.
http://dx.doi.org/10.1109/ICEAA65662.2025.11306007

N.B. When citing this work, cite the original published paper.

© 2025 IEEE. Personal use of this material is permitted. Permission from IEEE must be obtained for all other uses, in any current or future media, including reprinting/republishing this material for advertising or promotional purposes, or reuse of any copyrighted component of this work in other works.

(article starts on next page)

Domain Decomposition Analysis of Open-cavity-based Array Elements — Roadmap Toward Analyzing Large-Scale Reflectarrays and Reconfigurable Intelligent Surfaces

Rob Maaskant*, Dijun Lin*, Fitim Maxharraj*, Morteza Ghaderi Aram*,
Lars Manholm†, Parisa Aghdam†, Giampiero Gerini‡, Tommy Svensson*, Marianna Ivashina*
*Chalmers University of Technology, Chalmersplatsen 1, SE-412 96, Gothenburg, Sweden
{rob.maaskant,dijun,fitim,aramg,tommy.svensson,marianna.ivashina}@chalmers.se
†Ericsson Research, Lindholmspiren 11, 417 56, Gothenburg, Sweden
{lars.manholm,parisa.aghdam}@ericsson.com
‡TNO – Optics Department, Stieltjesweg 1, 2628 CK, Delft, The Netherlands
giampiero.gerini@tno.nl

***Abstract*—This paper describes a numerical modeling framework toward analyzing large-scale finite-sized reflectarrays and reconfigurable intelligent surfaces. A domain decomposition method (DDM) is proposed, where a single reflecting unit cell can be characterized in isolation from its embedded structure. The mutual coupling between unit cells is occurring only over-the-air and is modeled through a generalized admittance matrix approach. Both the radiated and scattered fields, which are computed for a transmitting and scattering problem, respectively, are in excellent agreement with those computed by CST Microwave Studio and a plain MoM approach. Recommendations and future directions are provided as part of the herein presented roadmap, among which the hybridization with fast methods and high-frequency techniques capable of handling the large-scale exterior domain, and the use of a finite difference/element method for modeling the interior domain of complex unit cells.**

***Index Terms*—Reflectarrays, multiscale structures, method of moments, reconfigurable antennas, metasurfaces.**

I. Introduction

THE research on reconfigurable intelligent surfaces (RIS) has grown tremendously in recent years due to their transformative potential in applications such as 5G and beyond wireless networks, radar systems, and electromagnetic wave control. These technologies promise enhanced performance, energy efficiency, and spatial reconfigurability [1].

The analysis of large-scale arrays typically assume periodic boundary conditions (PBC), by treating the array cells as part of an infinitely large periodic structure [2], [3]. An interesting example is the macroscale modeling of such arrays using ray-based approaches [4]. However, these approximations become inaccurate when the coupling between cells depends heavily on finite array effects or when the surface reflectivity becomes aperiodic.

To address these challenges, an efficient numerical approach that can accurately model mutual coupling and multiscale array effects is essential. Numerous studies have proposed frameworks that combine different techniques to handle these complexities [5]–[9]. The present paper contributes to this body of work by introducing a hybrid modeling framework, which synergistically integrates various methods to efficiently address these problems.

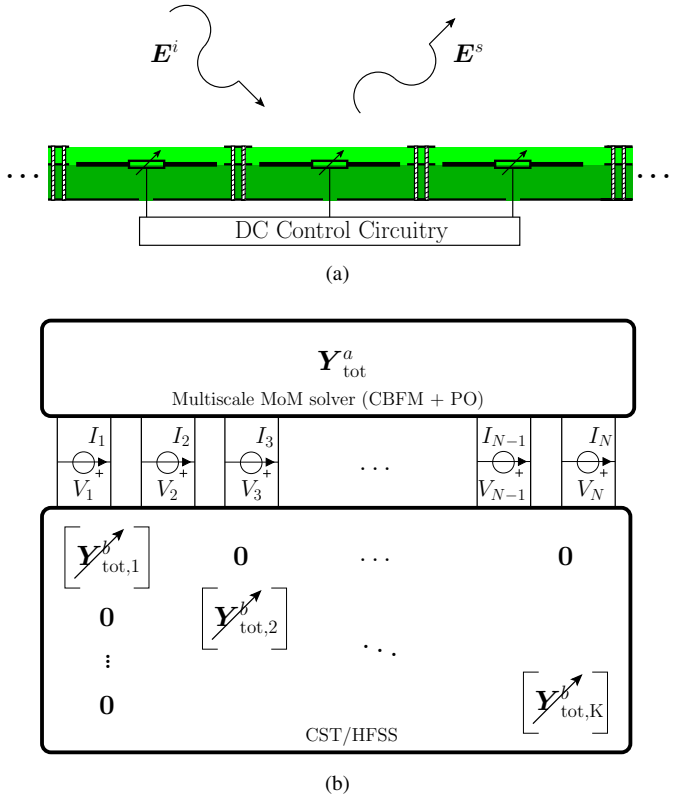


Fig. 1. (a) Printed circuit board employing via-fences to realize open-cavity-based reflectarray elements with backside control circuitry, and; (b) Generalized admittance matrix equivalent network representation for the multi-solver multi-mode domain decomposition method. A total of N aperture modes are distributed over K reflectarray cells.

The baseline reflectarray geometry in this study is shown

in Fig. 1(a), consisting of a (multilayer) printed circuit board (PCB). The PCB employs via-fences to create open-ended cavities that house the reconfigurable reflectarray elements. This way, the mutual coupling between reflectarray elements occurs only through over-the-air coupling, not via the substrate. This slight limitation in design flexibility significantly reduces the computational complexity of the problem, as we now can model the cells as metal cavities with apertures, distinguishing our approach from methods that model substrate-based coupling through open boundaries [5], [6].

Furthermore, each reflectarray cell can now be modeled independently from their surrounding environment through the use of surface equivalence principles. In fact, a null-field is assumed in the complementary/exterior domain. This leads to both electric and magnetic surface currents at the domain interface. The perfect electric conductor (PEC) boundary condition is imposed on this fictitious surface. Equivalent magnetic current only reside on apertures, not on metal boundaries; aperture field modes are modeled by corresponding magnetic currents, which are then used as a sources to construct a generalized admittance matrix for that domain. This is repeated for each domain after which the K cells and outer region domain are interconnected by interconnecting multiport admittance matrices in a circuit-like manner as shown in Fig. 1(b). The voltage at each port is the amplitude of the corresponding magnetic current modeling an aperture field mode. Fig. 1(b) shows N aperture magnetic currents/modes in total, thus N/K aperture modes per cell, provided that equal cells are used. Each aperture mode can be represented by an entire-domain basis function for modeling the respective magnetic current. This will drastically reduce the number of current modes relative to employing subsectional basis functions and suits the Characteristic Basis Function Method (CBFM) well [8]–[11].

Our method belongs to a class of so-called domain decomposition methods (DDMs). In most of the DDMs, such as the generalized transition matrix (GTM) approach [7], Love's equivalence principle is employed. It is often favored because it leads to well-conditioned numerical systems and integrates well with hybrid computational techniques. In our case, for the exterior equivalence, the entire array structure can be modeled as a PEC structure. Moreover, for large arrays the backside current is small, so that the PEC array of closed cavities can then be reduced to a PEC sheet. We can subsequently use high-frequency techniques, such as the Physical Optics (PO) approximation, to find the induced PEC current. In turn, the admittance matrix of each interior cavity domain can be characterized by a commercial solver employing a finite difference/element technique. Furthermore, by reducing the array of volumetric PEC cavities to a single sheet, it is believed that the relatively ill-conditioning of the proposed method, e.g. due to the interior resonance problem, will then be mitigated. The solver hybridization and geometrical dimension reduction as described above is subject of future study, but it is still mentioned here to motivate our currently preferred choice of equivalence principle. Also, the DDM as proposed in this paper will be at the heart of the RIS modeling framework and will be used to validate the integration of different solvers in the future. In terms of the hybridization of different solvers in a DDM context, the reader is kindly referred to [6].

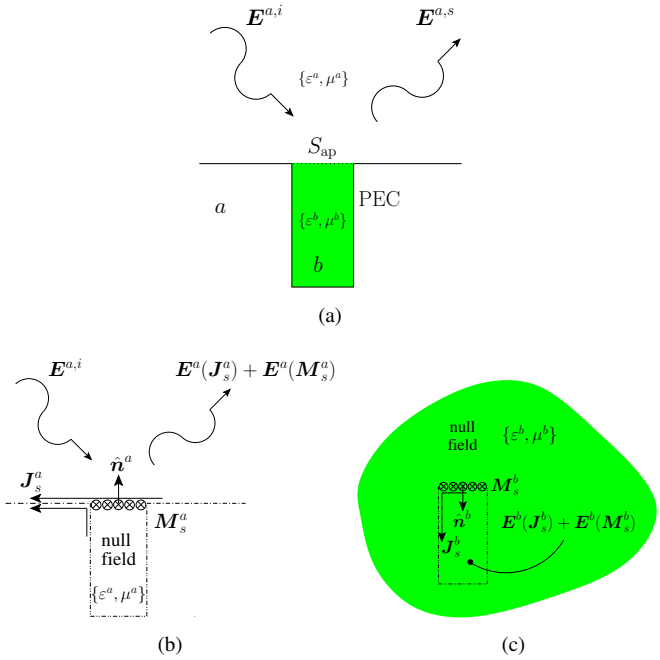


Fig. 2. Scattering problem: (a) Original configuration, split into: (b) exterior equivalent fields in region a; (c) interior equivalent fields in region b.

Finally, it is worth pointing out that the above-proposed DDM framework constitutes a valuable tool for optimizing the global response of active metasurfaces [12], [13]. It allows for the optimization of array configurations by leveraging a database of pre-characterized reconfigurable unit cells. Machine Learning techniques combined with optimization algorithms are then employed to optimize the distribution of these cells [14].

This paper is organized as follows. Sec. II details the mathematical formulation of the herein proposed DDM. The numerical results validating the methodology are described in Sec. III. The paper ends by providing the conclusions in Sec. IV.

II. Formulation

The present method is based on the generalized aperture admittance matrix approach as described in [15], albeit without the need to introduce a correction current.

In the original problem, in Fig. 2(a), the tangential components of the E- and H-fields are continuous *across the aperture* surface S_{ap}, i.e.,

$$\boldsymbol{E}^a\big|_{\text{tan}} = \boldsymbol{E}^b\big|_{\text{tan}} \quad \text{and} \quad \boldsymbol{H}^a\big|_{\text{tan}} = \boldsymbol{H}^b\big|_{\text{tan}}, \tag{1}$$

where a denotes the exterior region and b the interior waveguide region. For the exterior problem, in Fig. 2(b), we assume the original fields in region a and zero fields in region b. The jump in $\boldsymbol{E}^a\big|_{\text{tan}} = -\hat{\boldsymbol{n}}^a \times \hat{\boldsymbol{n}}^a \times \boldsymbol{E}^a$ must now be accompanied by an aperture surface magnetic current through the boundary condition $\boldsymbol{E}^a\big|_{\text{tan}} = \hat{\boldsymbol{n}}^a \times \boldsymbol{M}_s^a$. The jump in $\boldsymbol{H}^a\big|_{\text{tan}}$ leads to a surface electric current in the aperture. Furthermore, the PEC

surface is removed and replaced by an electric source current $\boldsymbol{J}_s^a$ representing the induced current across the exterior PEC surface as indicated in Fig. 2(b). The null-field interior region can now be filled with the exterior medium material a, so that all currents radiate in a homogeneous medium. The total exterior field in region a is therefore

$$\boldsymbol{E}^a = \boldsymbol{E}^{a,i} + \boldsymbol{E}^a(\boldsymbol{M}_s^a) + \boldsymbol{E}^a(\boldsymbol{J}_s^a) \tag{2a}$$
$$\boldsymbol{H}^a = \boldsymbol{H}^{a,i} + \boldsymbol{H}^a(\boldsymbol{M}_s^a) + \boldsymbol{H}^a(\boldsymbol{J}_s^a). \tag{2b}$$

Similarly, equivalence principles can be applied to obtain the total interior fields in region b, as also shown in Fig. 2(c), i.e.,

$$\boldsymbol{E}^b = \boldsymbol{E}^{b,i} + \boldsymbol{E}^b(\boldsymbol{M}_s^b) + \boldsymbol{E}^b(\boldsymbol{J}_s^b) \tag{3a}$$
$$\boldsymbol{H}^b = \boldsymbol{H}^{b,i} + \boldsymbol{H}^b(\boldsymbol{M}_s^b) + \boldsymbol{H}^b(\boldsymbol{J}_s^b), \tag{3b}$$

where the interior current $\boldsymbol{J}_s^b$ is different from the exterior current $\boldsymbol{J}_s^a$. However, because of Eq. (1), where

$$\boldsymbol{E}^{a,b}\big|_{\text{tan}} = \hat{\boldsymbol{n}}^{a,b} \times \boldsymbol{M}_s^{a,b} \tag{4}$$

as well as that $\hat{\boldsymbol{n}}^a = -\hat{\boldsymbol{n}}^b$ in the aperture, results in the single magnetic current

$$\boldsymbol{M}_s^a = -\boldsymbol{M}_s^b = \boldsymbol{M}_s. \tag{5}$$

An equation for $\boldsymbol{M}_s$ can be found by substituting (5) in both (3b) and (2b), and then in (1), yielding

$$\begin{aligned}&\big[\boldsymbol{H}^a(\boldsymbol{M}_s) + \boldsymbol{H}^b(\boldsymbol{M}_s)\big]_{\text{tan}} \\ &+ \big[\boldsymbol{H}^a(\boldsymbol{J}_s^a) - \boldsymbol{H}^b(\boldsymbol{J}_s^b)\big]_{\text{tan}} = \big[\boldsymbol{H}^{b,i} - \boldsymbol{H}^{a,i}\big|_{\text{tan}} \quad \boldsymbol{r} \in S_{\text{ap}},\end{aligned} \tag{6}$$

where $\boldsymbol{r}$ denotes the observation point. The exterior and interior currents $\boldsymbol{J}_s^{a,b}$ depend on $\boldsymbol{M}_s$. These relations follow from the E-field boundary conditions in (4), which must hold across the entire boundary surface, including the aperture. Note that, outside of the support of $\boldsymbol{M}_s$, the PEC boundary condition for the E-field is correctly enforced. The interior and exterior electric currents will be resolved first, after which the unknown current $\boldsymbol{M}_s$ is solved through (6).

Substituting (3a) and (2a) in (4) and using (5), gives the Electric Field Integral Equations (EFIE)

$$\big[\boldsymbol{E}^{a,i} + \boldsymbol{E}^a(\boldsymbol{M}_s) + \boldsymbol{E}^a(\boldsymbol{J}_s^a)\big]_{\text{tan}} = \hat{\boldsymbol{n}}^a \times \boldsymbol{M}_s \tag{7a}$$
$$\Big[\boldsymbol{E}^{b,i} - \boldsymbol{E}^b(\boldsymbol{M}_s) + \boldsymbol{E}^b(\boldsymbol{J}_s^b)\Big]_{\text{tan}} = -\hat{\boldsymbol{n}}^b \times \boldsymbol{M}_s. \tag{7b}$$

The current-dependent fields must be interpreted in terms of the integro-differential operators [17, Eq. (2.127)]:

$$\boldsymbol{H}^{a,b}(\boldsymbol{J}_s^{a,b}) = \mathcal{K}^{a,b}(\boldsymbol{J}_s^{a,b}) - \frac{1}{2}\hat{\boldsymbol{n}}^{a,b} \times \boldsymbol{J}_s^{a,b}, \tag{8}$$

where

$$\mathcal{K}^{a,b}(\boldsymbol{X}_s) = \int_S \boldsymbol{X}_s(\boldsymbol{r}') \times \boldsymbol{\nabla}' G^{a,b}(\boldsymbol{r} - \boldsymbol{r}')\,\mathrm{d}S', \tag{9}$$

and where the scalar Green's function for a homogeneous medium

$$G^{a,b}(\boldsymbol{r} - \boldsymbol{r}') = \frac{e^{-jk^{a,b}|\boldsymbol{r}-\boldsymbol{r}'|}}{4\pi|\boldsymbol{r} - \boldsymbol{r}'|}. \tag{10}$$

The wavenumber in the medium is given by its material constitutive parameters, i.e., $k^{a,b} = \omega\sqrt{\mu^{a,b}\varepsilon^{a,b}}$, and $\boldsymbol{r}'$ is a point in the source domain. Furthermore,

$$\boldsymbol{E}^{a,b}(\boldsymbol{J}_s^{a,b}) = \mathcal{L}^{a,b}(\boldsymbol{J}_s^{a,b}), \tag{11}$$

where

$$\begin{aligned}\mathcal{L}^{a,b}(\boldsymbol{X}) = &-j\omega\mu^{a,b}\int_S \boldsymbol{X}_s(\boldsymbol{r}')G^{a,b}(\boldsymbol{r} - \boldsymbol{r}')\,\mathrm{d}S' \\ &+ \frac{1}{j\omega\varepsilon^{a,b}}\boldsymbol{\nabla}\int_S \boldsymbol{\nabla}' \cdot \boldsymbol{X}(\boldsymbol{r}')G^{a,b}(\boldsymbol{r} - \boldsymbol{r}')\,\mathrm{d}S'.\end{aligned} \tag{12}$$

Finally, using duality,

$$\boldsymbol{H}^{a,b}(\boldsymbol{M}_s^{a,b}) = \frac{1}{\eta_{a,b}^2}\mathcal{L}^{a,b}(\boldsymbol{M}_s) \tag{13a}$$
$$\boldsymbol{E}^{a,b}(\boldsymbol{M}_s^{a,b}) = -\mathcal{K}^{a,b}(\boldsymbol{M}_s) + \frac{1}{2}\hat{\boldsymbol{n}}^{a,b} \times \boldsymbol{M}_s^{a,b}. \tag{13b}$$

These surface integrations need to be interpreted in the Cauchy principal value sense. The EFIEs in (7) are now written as

$$-\mathcal{L}^a(\boldsymbol{J}_s^a)\big|_{\text{tan}} = \big[-\mathcal{K}^a(\boldsymbol{M}_s) + \boldsymbol{E}^{a,i}\big]_{\text{tan}} - \frac{1}{2}\hat{\boldsymbol{n}}^a \times \boldsymbol{M}_s \tag{14a}$$
$$-\mathcal{L}^b(\boldsymbol{J}_s^b)\big|_{\text{tan}} = \big[\mathcal{K}^b(\boldsymbol{M}_s) + \boldsymbol{E}^{b,i}\big]_{\text{tan}} + \frac{1}{2}\hat{\boldsymbol{n}}^b \times \boldsymbol{M}_s \tag{14b}$$

for the exterior and interior electric surface currents, respectively, given an $\boldsymbol{M}_s$. We can solve the EFIEs through the method of moments using the following discretizations

$$\begin{aligned}\boldsymbol{J}_s^a(\boldsymbol{r}) &= \sum_{n=1}^{N^a} I_n^a \boldsymbol{i}_n^a(\boldsymbol{r}), \quad \boldsymbol{J}_s^b(\boldsymbol{r}) = \sum_{n=1}^{N^b} I_n^b \boldsymbol{i}_n^b(\boldsymbol{r}), \\ \boldsymbol{M}_s(\boldsymbol{r}) &= \sum_{n=1}^{N} V_n \boldsymbol{m}_n(\boldsymbol{r})\end{aligned} \tag{15}$$

Testing (14) by the basis functions $\{\boldsymbol{i}_m^{a,b}\}$, using the symmetric product $\langle \boldsymbol{a}, \boldsymbol{b}\rangle = \int \boldsymbol{a} \cdot \boldsymbol{b}\,dS$, yields

$$\sum_{n=1}^{N^a} Z_{mn}^a I_n^a = \sum_{n=1}^{N} D_{mn}^a V_n + V_m^{a,i} \tag{16}$$
$$\sum_{n=1}^{N^b} Z_{mn}^b I_n^b = -\sum_{n=1}^{N} D_{mn}^b V_n + V_m^{b,i} \tag{17}$$

for $m = 1, 2, \ldots, N^{a,b}$, respectively, where

$$Z_{mn}^{a,b} = -\langle \boldsymbol{i}_m^{a,b}, \mathcal{L}^{a,b}(\boldsymbol{i}_n^{a,b})\rangle \tag{18a}$$
$$D_{mn}^{a,b} = -\langle \boldsymbol{i}_m^{a,b}, \mathcal{K}^{a,b}(\boldsymbol{m}_n)\rangle - \frac{1}{2}\langle \boldsymbol{i}_m^{a,b}, \hat{\boldsymbol{n}}^{a,b} \times \boldsymbol{m}_n\rangle \tag{18b}$$
$$V_m^{a,i} = \langle \boldsymbol{i}_m^a, \boldsymbol{E}^{a,i}\rangle \quad \text{and} \quad V_m^{b,i} = \langle \boldsymbol{i}_m^b, \boldsymbol{E}^{b,i}\rangle, \tag{18c}$$

or simply

$$\mathbf{Z}^a\mathbf{I}^a = \mathbf{D}^a\mathbf{V} + \mathbf{V}^{a,i} \tag{19a}$$
$$\mathbf{Z}^b\mathbf{I}^b = -\mathbf{D}^b\mathbf{V} + \mathbf{V}^{b,i}. \tag{19b}$$

Thus, the solution becomes

$$\mathbf{I}^a = (\mathbf{Z}^a)^{-1}\left(\mathbf{V}^{a,i} + \mathbf{D}^a\mathbf{V}\right) \tag{20a}$$
$$\mathbf{I}^b = (\mathbf{Z}^b)^{-1}\left(\mathbf{V}^{b,i} - \mathbf{D}^b\mathbf{V}\right). \tag{20b}$$

Similarly, applying the same discretization process to the Magnetic Field Integral Equation (MFIE) in (6) and testing by the basis functions $\{\boldsymbol{m}_m\}$, yields

$$\sum_{n=1}^{N}\left[Y_{mn}^{a}+Y_{mn}^{b}\right]V_n + \sum_{n=1}^{N^b} C_{mn}^{b} I_n^b - \sum_{n=1}^{N^a} C_{mn}^{a} I_n^a = I_m^{a,i} - I_m^{b,i}, \quad (21)$$

where

$$Y_{mn}^{a,b} = -\frac{1}{\eta_{a,b}^2}\langle \boldsymbol{m}_m, \mathcal{L}^{a,b}(\boldsymbol{m}_n)\rangle \quad (22a)$$

$$C_{mn}^{a,b} = \langle \boldsymbol{m}_m, \mathcal{K}^{a,b}(\boldsymbol{i}_n^{a,b})\rangle - \frac{1}{2}\langle \boldsymbol{m}_m, \hat{\boldsymbol{n}}^{a,b}\times \boldsymbol{i}_n^{a,b}\rangle \quad (22b)$$

$$I_m^{a,i} = \langle \boldsymbol{m}_m, \boldsymbol{H}^{a,i}\rangle \quad \text{and} \quad I_m^{b,i} = \langle \boldsymbol{m}_m, \boldsymbol{H}^{b,i}\rangle, \quad (22c)$$

or simply

$$\left[\mathbf{Y}^a + \mathbf{Y}^b\right]\mathbf{V} + \mathbf{C}^b\mathbf{I}^b - \mathbf{C}^a\mathbf{I}^a = \mathbf{I}^{a,i} - \mathbf{I}^{b,i}. \quad (23)$$

One can now substitute (20) in (23) to finally arrive at

$$\left[\mathbf{Y}_{\text{tot}}^a + \mathbf{Y}_{\text{tot}}^b\right]\mathbf{V} = \mathbf{I}, \quad (24)$$

where

$$\mathbf{Y}_{\text{tot}}^a = \mathbf{Y}^a - \mathbf{C}^a(\mathbf{Z}^a)^{-1}\mathbf{D}^a \quad (25a)$$

$$\mathbf{Y}_{\text{tot}}^b = \mathbf{Y}^b - \mathbf{C}^b(\mathbf{Z}^b)^{-1}\mathbf{D}^b \quad (25b)$$

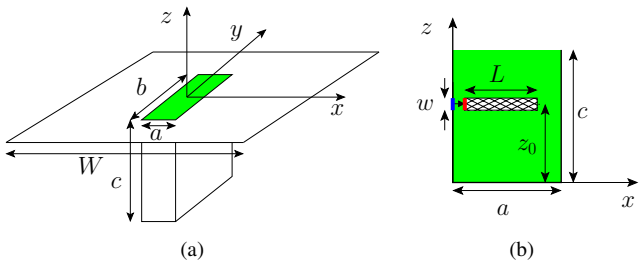
$$\mathbf{I} = \left[\mathbf{I}^{a,i} + \mathbf{C}^a(\mathbf{Z}^a)^{-1}\mathbf{V}^{a,i}\right] - \left[\mathbf{I}^{b,i} + \mathbf{C}^b(\mathbf{Z}^b)^{-1}\mathbf{V}^{b,i}\right], \quad (25c)$$

and where the matrix elements are computed using (22) and (18). Once $\mathbf{V}$ is solved for an incident field $\mathbf{I}$, the exterior magnetic current $\boldsymbol{M}_s$ is known through the basis function expansion (15), as well as the exterior electric current $\boldsymbol{J}_s^a$ through the expansion coefficient vector (20a). These currents radiate the exterior scattered field in a homogeneous medium $\{\mu^a, \varepsilon^a\}$, and together with the incident field, the total field is obtained as per (2a). Note how Fig. 1(b) visualizes Eq. (24), with the difference that the voltage sources are now replaced by current sources that are dependent on the field excitation.

III. Numerical Results

For the purpose of validation, consider the rectangular waveguide element in Fig. 3(a). The element is of size $a\times b\times c$, where its aperture opening is in the $z = 0$ PEC ground plane. The ground plane is of size $W \times W$. We consider two scenarios: (i) a dielectric filled waveguide ($\varepsilon_{\text{r}} = 2.2$) considered in the transmitting situation that is excited by a monopole PEC feed as shown in Fig. 3(b), and; (ii) a 2×1 reflectarray of empty air-filled waveguides, excited by a Huygens point source placed along the z-axis and radiating into the negative z-direction.

Our objective is to validate the DDM-computed input impedance and radiation pattern for the probe-excited waveguide using both CST Microwave Studio (2020) and a plain EFIE approach. Additionally, the DDM-computed scattering characteristics of the 2×1 reflectarray are compared to a plain MoM approach (EFIE only). In all our simulations we have



(a) (b)

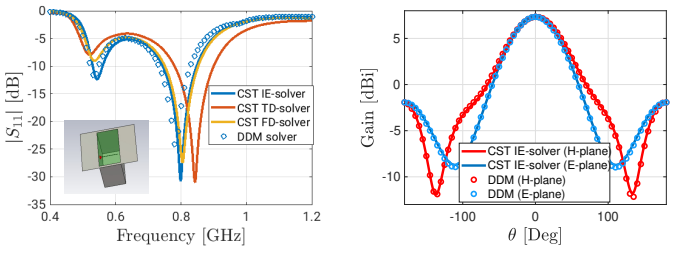
a	b	c	W	L	w	z_0	ϵ_{r}
9	21	12	23.1	7.5	0.1	7.5	2.2

Fig. 3. Dimensions in cm: (a) Open waveguide; (b) Monopole strip and port.

employed Rao-Wilton-Glisson (RWG) basis and test functions (Gelerkin's approach) for both the electric and magnetic currents.

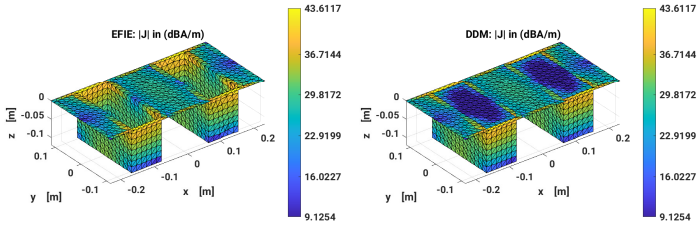
One can conclude from Fig. 4(a) that the magnitude of the port reflection coefficient $|S_{11}|$ as computed by CST's integral solver, time-domain solver, and frequency-domain solver are in good agreement with our proposed DDM results. The shift in resonance frequency is seen to be dependent on CST's solver type (default solver and mesh settings are used). CST's integral equation (IE) solver agrees best with our MoM-based DDM. Furthermore, the E- and H-field radiation patterns in Fig. 4(b) are visually almost indistinguishable from the DDM-computed patterns. Note that only CST's IE-solver patterns results are shown, since CST's other solvers yield visually identical patterns and are therefore omitted. The DDM mesh density is $\lambda/12$ @1 GHz. At this high mesh density the predicted resonance frequency is only weakly dependent on the mesh. The results generally confirm that the proposed DDM is working as expected.

Next, the 2×1 reflectarray in Fig. 5 is considered. A Huygens point source with unity electric dipole moment $\hat{\boldsymbol{x}}$ [Am] and magnetic dipole moment $-\eta_a\hat{\boldsymbol{y}}$ [Vm] are placed at $(x = 0, y = 0, z = \lambda)$ and radiates in the negative z-direction. The reference induced surface current is shown in Fig. 5(a) as computed by a plain MoM approach (EFIE only). The induced electric surface current as computed by the DDM is shown in Fig. 5(b). The exterior and interior current are summed to form the total electric current, so that this total current in Fig. 5(b) can be compared to the MoM current in Fig. 5(a). The current distributions agree very well, despite that



(a) (b)

Fig. 4. DDM vs. CST radiation characteristics comparison: (a) Port reflection coefficient; (b) Power pattern in two principal planes @0.85 GHz.



(a) (b)

Fig. 5. Current distribution of 2×1 array of air-filled waveguides as computed by the DDM and a plain EFIE approach (a) EFIE current; (b) DDM current.

the total electric current in the aperture in Fig. 5(b) does not fully vanish. The latter, however, does not have a detrimental effect on the E- and H-plane scattering patterns as shown in Fig. 6(a). The relative pattern error is computed as

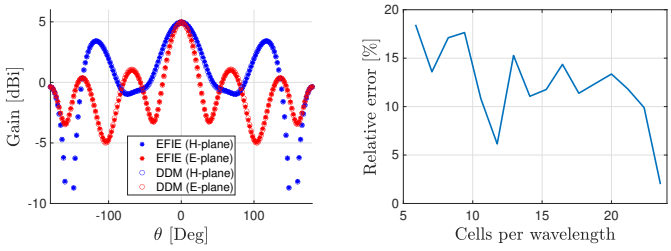
$$\epsilon = \frac{\left\|\mathbf{U}^{\text{EFIE}} - \mathbf{U}^{\text{DDM}}\right\|_{\text{Fro}}}{\left\|\mathbf{U}^{\text{EFIE}}\right\|_{\text{Fro}}} \times 100\% \tag{26}$$

where "Fro" denotes the Frobenius norm and where $\mathbf{U}$ is a vector of uniformly sampled radiation intensities across a far-field sphere.

We noticed that an unusually dense mesh had to be taken to get accurate results, as shown in Fig. 6(b). This may be due to the non-vanishing aperture current in Fig. 5(b), requiring a denser mesh near the edges. Furthermore, MATLAB issued a high condition number warning for the densest mesh ($\lambda/24$). This may be attributed to the well-known interior resonance problem this formulation is susceptible to. We expect not to have this problem in the future, since large reflectarrays will have negligible current on the backside, so that the potentially resonant cavities can be removed when solving the exterior problem as a sheet problem, which also significantly alleviates the computational complexity. For the interior problem we will then use a commercial solver (CST/HFSS), enabling us to model more complex and realistic unit cells. The DDM as presented in this paper will be used to interconnect the multi-solver domains and also to validate the overall obtained solution.

IV. Conclusion

A domain decomposition method for open-cavity based reflectarrays is proposed. The surface equivalence principle is employed to model the exterior problem as a full metal structure for which, in the future, fast methods can be used (e.g. CBFM + PO). Furthermore, if the backside current can be neglected, it is believed that the exterior structure may even be reduced to a metal sheet. The interior problem (i.e. the reflectarray element) is characterized by a generalized admittance matrix through an in-house MoM solver. The present paper has shown that the domains, each of which is characterized by a generalized admittance matrix, can be interconnected in a circuit-type manner. The overall array response has been validated for: (i) a radiating dielectric-filled waveguide, and; (ii) a 2×1 reflectarray element with Huygens source excitation. The successful validation with CST and a plain MoM approach of both the radiation and scattering characteristics show that the proposed DDM approach can serve as the future interface for connecting commercial field solvers to fast integral-equation based methods for solving large-scale reflectarray and reconfigurable intelligent surface problems. This hybrid solution method will also eliminate the interior resonance problem that the current formulation is susceptible to.



(a) (b)

Fig. 6. (a) Comparison EFIE vs. DDM of E- and H-plane gain pattern; (b) 3-D pattern error for DDM as a function of mesh density relative to reference solution (EFIE with $\lambda/24$ mesh density).

Acknowledgments

This work was funded by the European Union, under ANTERRA 101072363 HORIZON-MSCA-2021-DN-01. Views and opinions expressed are however those of the author(s) only and do not necessarily reflect those of the European Union. Neither the European Union nor the granting authority can be held responsible for them.

Furthermore, it is supported by the WiTECH Centre (DigiArray & DisCourSe projects), which is financed by VINNOVA, Ericsson, Saab, Satcube, and Chalmers in Sweden.

Finally, this work is sponsored by the Dutch National Growth Fund project "6G Future Network Services (FNS)".

References

[1] Y. Zhao, "Reconfigurable intelligent surfaces for 6G: applications, challenges, and solutions," *Front Inform Technol Electron Eng*, vol. 24, pp. 1669-–1688, 2023.

[2] Wei Huang, Mai Liu, Yi Xu, Shan Yin, Wentao Zhang, and Jiaguang Han, "Huygens principle for random metamaterial without coupling," *J. Opt. Soc. Am. B* vol. 40, no. 2, 312–317, 2023.

[3] E. Baladi and S. V. Hum, "Equivalent Circuit Models for Metasurfaces Using Floquet Modal Expansion of Surface Current Distributions," *IEEE Trans. Antennas Propag.*, vol. 69, no. 9, pp. 5691–5703, Sept. 2021.

[4] V. Degli-Esposti, E. M. Vitucci, M. D. Renzo and S. A. Tretyakov, "Reradiation and Scattering From a Reconfigurable Intelligent Surface: A General Macroscopic Model," *IEEE Trans. Antennas Propag.*, vol. 70, no. 10, pp. 8691–8706, Oct. 2022.

[5] R. Gholami, P. Naseri, P. Triverio and S. V. Hum, "An Efficient Integral Equation Method for Full-Wave Analysis of Inhomogeneous Electromagnetic Surfaces With Connected Conductors," *IEEE Trans. Antennas Propag.*, vol. 70, no. 7, pp. 5647–5658, Jul. 2022.

[6] M. Jiang et al., "Efficient and Accurate Simulations of Metamaterials Based on Domain Decomposition and Unit Feature Database," *IEEE Trans. Antennas Propag.*, vol. 72, no. 11, pp. 8635–8646, Nov. 2024.

[7] Y. Hu, G. Xiao, R. Liu and S. Huang, "A Generalized Transition Matrix Model for Dielectric Coated PEC Cavities," *IEEE MTT-S International Wireless Symposium (IWS)*, Shanghai, China, pp. 1–3, 2020.

[8] H. Shao, K. Fu, Z. Fu, X. Ying and J. Hu, "A Fast Model Order Reduction Method for Electromagnetic Scattering of Large Periodic Arrays With Connected Elements," *IEEE Trans. Antennas Propag.*, vol. 71, no. 11, pp. 9142–9147, Nov. 2023.

[9] I. Kim, H. -R. Im, I. -P. Hong, H. Lee and J. -G. Yook, "An Accelerated Method of a Generalized Transition Matrix Model Using Characteristic Basis Functions for Large-Scale Open-Ended Cavities," *IEEE Trans. Antennas Propag.*, vol. 72, no. 8, pp. 6813–6818, Aug. 2024.

[10] J. F. Gao and F. H. Lin, "Modeling and Analysis of Wideband Multilayer Metasurface Antenna Array Using Characteristic-Mode Analysis," *IEEE Trans. Antennas Propag.*, vol. 71, no.3, pp. 2832–2836, Mar. 2023.

[11] R. Maaskant, "Analysis of large antenna systems," Phd Thesis, Technische Universiteit Eindhoven (TUe), 2010.

[12] Z. Zhang et al., "Macromodeling of Reconfigurable Intelligent Surface Based on Microwave Network Theory," *IEEE Trans. Antennas Propag.*, vol. 70, no. 10, pp. 8707–8717, Oct. 2022.

[13] J. W. Zhang et al., "A Novel Two-Stage Optimization Framework for Designing Active Metasurfaces Based on Multiport Microwave Network Theory," *IEEE Trans. Antennas Propag.*, vol. 72, no. 2, pp. 1603–1616, Feb. 2024.

[14] Y. Ma, J. F. Kolb, A. A. Ihalage, A. S. Andy and Y. Hao, "Incorporating Meta-Atom Interactions in Rapid Optimization of Large-Scale Disordered Metasurfaces Based on Deep Interactive Learning," *Adv. Photonics Res.*, 4: 2200099.

[15] T. Wang, R. F. Harrington and J. R. Mautz, "Electromagnetic scattering from and transmission through arbitrary apertures in conducting bodies," *IEEE Trans. Antennas Propag.*, vol. 38, no. 11, pp. 1805–1814, Nov. 1990.

[16] R. F. Harrington, *Time-harmonic electromagnetic fields*, New York : McGraw Hill, 1961.

[17] W. C. Gibson, *The method of moments in electromagnetics*, Chapman and Hall/CRC, 2021.